Compensation and Alignment of Thermohaline Gradients in the Ocean Mixed Layer

RAFFAELE FERRARI

Massachusetts Institute of Technology, Cambridge, Massachusetts

FRANCESCO PAPARELLA*

Scripps Institution of Oceanography, La Jolla, California

(Manuscript received 10 February 2003, in final form 24 April 2003)

ABSTRACT

The surface mixed layer of the ocean is often characterized by thermohaline compensation and alignment. That is, temperature and salinity gradients tend to be parallel and to cancel in their contribution to density. In this paper a combination of theoretical arguments and numerical simulations is presented to investigate how compensation and alignment emerge as a result of processes at work within the mixed layer. The dynamics of the mixed layer is investigated through a simple model that couples a nonlinear diffusive parameterization for the horizontal transports of temperature and salinity with stirring by mesoscale eddies. It is found that stirring quickly aligns the temperature and salinity gradients and that nonlinear diffusion creates compensation. Neither process, by itself, is sufficient to reproduce the observations.

1. Introduction

Observations show that the thermohaline structure of the surface mixed layer of the ocean is characterized by *thermohaline alignment* and *density compensation.* That is, temperature and salinity gradients tend to be parallel and to oppose each other in their effect on density. Thermohaline alignment is evident in frontal regions on scales of hundreds of kilometers (see, e.g., Roden 1975, 1977; Belkin 1996) and in a few high-resolution surveys on scales of tens of kilometers (Flament et al. 1985; Rudnick and Luyten 1996). Density compensation has been observed on large scales for decades (Roden 1975; Niiler 1984). Recent high-resolution observations have found compensation down to scales of tens of meters in the North Pacific (Rudnick and Ferrari 1999; Ferrari and Rudnick 2000) and throughout the global ocean on scales of kilometers (Rudnick and Martin 2002).

Young (1994) and Ferrari and Young (1997) suggest that compensation is the result of the selective diffusion of horizontal density gradients. This happens because the combined action of unbalanced motions and vertical mixing rapidly removes density gradients but leaves behind compensated temperature and salinity gradients. Unbalanced motions arise in the mixed layer (ML) because horizontal density fluctuations can be so large as to become gravitationally unstable. The physics of compensation can be described in an initial value problem. Assume that at time $t = 0$ atmospheric forcing creates random fluctuations of temperature and salinity in the ML. During the first stages of the rundown, the unbalanced motions remove all density gradients. The compensated gradients instead persist for much longer times. The argument is very appealing, but a question remains as to whether the selective diffusion of density gradients by this mechanism is fast enough to compete with the other processes at work in the ML, like horizontal stirring due to mesoscale motions, heat and freshwater surface fluxes, and entrainment of thermocline waters.

In this paper we revisit the work of Ferrari and Young by coupling a set of nonlinear diffusion equations, which parameterize the effect of unbalanced motions on density gradients, with a simple model of horizontal advection and thermohaline forcing by the sea surface fluxes. We show that advection speeds up the process of compensation by exponentially increasing density gradients until they are removed by unbalanced motions. Thus compensation is not a transient effect, but it is maintained in the presence of stirring and forcing, as it is the case in the real ML.

The paper is organized as follows. In section 2 we revisit the arguments of Young and collaborators for the parameterization of diapycnal fluxes in the ML. In section 3, we describe the numerical model used to test the

* Additional affiliation: Università di Lecce, Lecce, Italy.

Corresponding author address: Raffaele Ferrari, Bldg. 54-1420, Department of Earth, Atmospheric, and Planetary Sciences, Massachusetts Institute of Technology, 77 Massachusetts Avenue, Cambridge, MA 02139-4307.
E-mail: rferrari@mit.edu

nonlinear diffusive parameterization of heat and salt transports in the ML. In section 4, we use numerical simulations to investigate the physics of alignment and compensation of thermohaline gradients. Discussion and conclusions are in section 5.

2. Diffusive parameterization of eddy transfer of heat and salt in the mixed layer

Let us consider the dispersion of a tracer of concentration θ in the surface ML of the ocean. We model the ML as a vigorously mixed, shallow layer with a small aspect ratio, that is, with a depth H much less than the horizontal scale.

The transport of the tracer θ stirred by an incompressible velocity field $\mathbf{u}$ is described by the familiar advection–diffusion equation,

$$\partial_t\theta + \mathbf{u}\cdot\boldsymbol{\nabla}\theta = \mathcal{D}, \tag{1}$$

together with appropriate boundary conditions. If the diffusion operator is $\mathcal{D} = \kappa\nabla^2\theta$, where κ is the molecular diffusivity, (1) describes all scales of motion from a few millimeters to thousands of kilometers. By averaging in space and time it is sometimes possible to derive advection–diffusion equations where the details of the small-scale turbulent motions are hidden within a suitable operator $\mathcal{D}$. A natural choice for the ML is to average vertically over the depth H of the ML and over the characteristic time of vertical mixing τ_V. In the horizontal direction the averages are carried out on lengths not less than H. By decomposing θ and $\mathbf{u}$ into means, $\overline{\theta}$ and $\overline{\mathbf{u}}$, and in departures from those means, θ' and $\mathbf{u}'$, we obtain the Reynolds-averaged equation

$$\partial_t\overline{\theta} + \overline{\mathbf{u}}\cdot\boldsymbol{\nabla}\overline{\theta} = -\boldsymbol{\nabla}\cdot\overline{\mathbf{u}'\theta'} + \kappa\nabla^2\overline{\theta} + \mathcal{F}. \tag{2}$$

The term $\mathcal{F}$ represents sources and sinks of tracer induced by the boundary conditions at the top and bottom of the ML. From now on, derivatives are taken only in the horizontal because the averaged quantities do not depend on the vertical coordinate.

Prandtl proposed a mixing length hypothesis to obtain a turbulent closure and express the *eddy flux divergence*, the first term in the right-hand side of (2), in terms of mean quantities. The argument assumes that turbulent tracer fluxes can be characterized as a characteristic velocity $\mathbf{U}$ times a characteristic tracer fluctuation, given by the product of a mixing length $\mathbf{L}$ and the large-scale tracer gradient. In tensor notation, the eddy flux is then expressed as $\overline{\mathbf{u}'\theta'} = -\overline{\mathbf{U}\otimes\mathbf{L}}\boldsymbol{\nabla}\overline{\theta}$, where the dyadic product is the *eddy diffusivity*. In the special case of homogeneous and isotropic turbulent flows, the eddy diffusivity tensor is a constant $K \gg \kappa$. This closure is commonly used in models of the ocean ML, where temperature and salinity are diffused horizontally with a constant K independently of each other.

However, at scales larger than H, the ML eddy fluxes are driven mostly by horizontal inhomogeneities of the buoyancy field B.[1] Therefore the transport of tracer depends on the direction and the magnitude of $\boldsymbol{\nabla}B$. At small scales, where rotation is not important, it is reasonable to argue that $\mathbf{U}$ increases with $\boldsymbol{\nabla}\overline{B}$ and that $\mathbf{L} \propto \mathbf{U}\tau_V$, where τ_V is some characteristic time over which the ML is mixed in the vertical. Thus the flux-mean gradient relationship must be of the form

$$\overline{\mathbf{u}'\theta'} = -\gamma f(|\boldsymbol{\nabla}\overline{B}|)(\boldsymbol{\nabla}\overline{B}\cdot\boldsymbol{\nabla}\overline{\theta})\boldsymbol{\nabla}\overline{B}, \tag{3}$$

where γ is a positive constant that measures the intensity of the vertical mixing and $f(|\boldsymbol{\nabla}\overline{B}|)$ is a nondimensional, semidefinite-positive function, whose form depends on the details of the hydrodynamic instabilities that dominate in the eddy field. In the case of slumping buoyancy gradients, Ferrari and Young (1997) find $f(|\boldsymbol{\nabla}\overline{B}|) = 1$, which is what we shall use from now on. Notice that, even though the flux is in the direction of $\boldsymbol{\nabla}\overline{B}$, $\overline{\mathbf{u}'\theta'}\cdot\boldsymbol{\nabla}\overline{\theta} < 0$; thus the flux of tracer never goes up the mean gradient. However, only the projection of the tracer gradient along the direction of the buoyancy gradient contributes to the flux.

Closures of the same functional form given in (3) have been proposed to describe the tracer fluxes produced at baroclinically unstable fronts (Green 1970; Stone 1972; Pavan and Held 1996; Visbeck et al. 1997). In those models the closure represents the divergent component of the eddy fluxes.

We apply the closure in (3) to describe the dispersion of heat and salt in the ML. We assume a linear equation of state and measure T and S with the same units of buoyancy so that $B = T - S$. Neglecting the fluxes due to molecular diffusivity and dropping overbars one can add and subtract the equations for T and S to get the following equations for B and for the variable $V = T + S$:

$$\partial_t B + \mathbf{u}\cdot\boldsymbol{\nabla}B = \gamma\boldsymbol{\nabla}\cdot[(\boldsymbol{\nabla}B\cdot\boldsymbol{\nabla}B)\boldsymbol{\nabla}B] + \mathcal{F}_T - \mathcal{F}_S, \tag{4}$$

$$\partial_t V + \mathbf{u}\cdot\boldsymbol{\nabla}V = \gamma\boldsymbol{\nabla}\cdot[(\boldsymbol{\nabla}V\cdot\boldsymbol{\nabla}B)\boldsymbol{\nabla}B] + \mathcal{F}_T + \mathcal{F}_S. \tag{5}$$

Here $\mathcal{F}_T$ and $\mathcal{F}_S$ are the forcings on T and on S. The quantity V, first introduced by Veronis (1972), was named "spice" by Munk (1981). Spice is a passive scalar, in the case of a linear equation of state, because it has no feedbacks on either the advective or the diffusive fluxes.

The main characteristic of nonlinear diffusion is that it always dissipates buoyancy, even more so when $|\boldsymbol{\nabla}B|$ is large. Instead, in regions with small $|\boldsymbol{\nabla}B|$, but large spice gradients, $\boldsymbol{\nabla}V$ can persist for long times. The consequence of this selective decay is that, on average, spice gradients are larger than buoyancy ones. In terms of temperature and salinity, this means that $\boldsymbol{\nabla}T$ and $\boldsymbol{\nabla}S$ compensate in their effect on buoyancy; that is $\boldsymbol{\nabla}T \approx \boldsymbol{\nabla}S$ (Ferrari and Young 1997).

[1] Buoyancy B is defined as $\rho = \rho_0(1 - g^{-1}B)$, where ρ is the fluid's density field, ρ_0 is a constant reference density, and g is the acceleration of gravity.

TABLE 1. Parameters used in the numerical simulations: L_0 is the scale of the forcing in the equation for vorticity, $\mathcal{F}_T$ and $\mathcal{F}_S$ are the forcing functions that appear on the rhs of the equations for temperature and salinity, respectively, γ is the coefficient in front of the nonlinear diffusion term, κ is the coefficient in front of the linear hyperdiffusivity, and N is the number of grid points in x and in y. The resolution is the same in all simulations: $\Delta x = \Delta y = 0.1$ km.

	L_0 (km)	$\mathcal{F}_T$ (km h^{-3})	$\mathcal{F}_S$ (km h^{-3})	γ (km^2 h^3)	N
L1	6.4	$4 \times 10^{-2} \cos\left(\frac{2\pi}{51.2}x\right)$	$4 \times 10^{-2} \sin\left(\frac{2\pi}{51.2}y\right)$	0	512
L2	0.3	$4 \times 10^{-2} \cos\left(\frac{2\pi}{51.2}x\right)$	$4 \times 10^{-2} \sin\left(\frac{2\pi}{51.2}y\right)$	0	512
NL1	6.4	$4 \times 10^{-2} \cos\left(\frac{2\pi}{51.2}x\right)$	$4 \times 10^{-2} \sin\left(\frac{2\pi}{51.2}x\right)$	0.02	512
NL2	6.4	$8 \times 10^{-2} \cos\left(\frac{2\pi}{51.2}x\right)$	$4 \times 10^{-2} \cos\left(\frac{2\pi}{51.2}y\right)$	0.02	512
NL3	0.3	$4 \times 10^{-2} \cos\left(\frac{2\pi}{51.2}x\right)$	$4 \times 10^{-2} \sin\left(\frac{2\pi}{51.2}x\right)$	0.02	512
NL4	1	$5 \times 10^{-2} \cos\left(\frac{2\pi}{51.2}x\right)$	$5 \times 10^{-2} \sin\left(\frac{2\pi}{51.2}x\right)$	0.002	128
NL5	1	$5 \times 10^{-2} \cos\left(\frac{2\pi}{51.2}x\right)$	$5 \times 10^{-2} \sin\left(\frac{2\pi}{51.2}x\right)$	0.005	128
NL6	1	$5 \times 10^{-2} \cos\left(\frac{2\pi}{51.2}x\right)$	$5 \times 10^{-2} \sin\left(\frac{2\pi}{51.2}x\right)$	0.02	128
NL7	1	$5 \times 10^{-2} \cos\left(\frac{2\pi}{51.2}x\right)$	$5 \times 10^{-2} \sin\left(\frac{2\pi}{51.2}x\right)$	0.05	128
NL8	1	$5 \times 10^{-2} \cos\left(\frac{2\pi}{51.2}x\right)$	$5 \times 10^{-2} \sin\left(\frac{2\pi}{51.2}x\right)$	0.2	128

3. Numerical integration of the thermohaline equations

We illustrate the mechanisms of thermohaline alignment and compensation through numerical integrations of (4) and (5). The advective field is generated by solving the equations for the f-plane barotropic model with infinite Rossby radius of deformation,

$$\omega_t + J(\psi, \omega) = -\mu\omega + \nu\nabla^6\omega + \mathcal{F}_\omega \text{ and}$$
$$\omega = \nabla^2\psi, \tag{6}$$

where ω is the relative vorticity, ψ is the streamfunction, and J is the Jacobian operator. The velocity is related to the streamfunction as $\mathbf{u} = (-\partial_y\psi, \partial_x\psi)$. Dissipation is represented as a third-order harmonic operator (∇^6) that parameterizes subgrid-scale dissipation of vorticity and a bottom drag that prevents a pileup of kinetic energy in the lowest modes. This choice is common in simulations of turbulence (Salmon 1998). The diffusivities are set to $\mu = 2 \times 10^{-2}$ h^{-1} $\approx 6 \times 10^{-6}$ s^{-1} and $\nu = 2 \times 10^{-9}$ km^6 h^{-1} $\approx 6 \times 10^5$ m^6 s^{-1}. A standard Fourier–Galerkin pseudospectral method is used with integrating factor and circular dealiasing truncation with a cutoff radius of 8/9 of the Nyquist wavenumber (Canuto et al. 1987). The integration domain of 51.2×51.2 km^2 is biperiodic with a grid step $\Delta x = 0.1$ km. Time is advanced using a third-order Adams–Bashforth scheme with a time step $\Delta t = 0.01$ h. The vorticity equation is forced by adding a constant vorticity per unit time at a fixed scale; that is, $\mathcal{F}_\omega$ represents a constant $\Delta\Omega$ added to the vorticity spectrum at a wavenumber $\mathbf{k} = (k_x, k_y)$ having $|\mathbf{k}| = 2\pi/L_0$ and phase changed randomly every time step. The values of L_0, given in Table 1, are chosen case by case to investigate either the direct enstrophy cascade or the inverse energy cascade regimes of 2D turbulence (Salmon 1998). For simulations in the direct enstrophy cascade, coherent vortices form with a diameter that is approximately one-half of the forcing scale. Computational feasibility limits our result to examples with vortices of small size ($\sim$10 km). However, the numerical value of the eddy containing scale is not a major issue in the present analysis. The analysis focuses on submesoscale dynamics, and we draw conclusions only from what happens at scales well within the inertial range of the simulations. Increasing the size of the vortices to more appropriate oceanic values ($\sim$40 km) would only extend the range of scales over which our results apply.

The advective part of (4) and (5) is solved with the same scheme used for the vorticity equation (6). In simulations L1 and L2 (cf. Table 1) temperature and salinity are treated as independent passive scalars, that is, we set γ equal to zero. For these simulations we add a Laplacian diffusion operator with a diffusivity chosen such as to obtain a dissipation (Batchelor's) scale $L_{\text{diss}} \approx 0.23$ km. Simulations NL1–NL8 solve the full equa-

tions (4) and (5). The stiff nonlinear diffusion term is advanced in time by performing 10 predictor–corrector steps for each advective Adams–Bashforth step. Dealiasing truncation is complemented with a third-order hyperdiffusion, $\kappa\nabla^6 B$ and $\kappa\nabla^6 V$ respectively, with $\kappa = 2 \times 10^{-9}$ km^6 h^{-1}. The functional form of the forcing on temperature and salinity is specified in Table 1. Its amplitude is chosen such as to obtain temperature fluctuations of the order of 0.01°C across 100 m, a typical value for the ML. In all simulations, buoyancy and spice are set to zero at time $t = 0$, while vorticity starts from a statistically steady state.

4. Alignment and compensation of thermohaline gradients

Correlations between temperature and salinity gradients are commonly quantified along one-dimensional paths in terms of the density ratio

$$R_{1D} \equiv \frac{\hat{\ell} \cdot \boldsymbol{\nabla} T}{\hat{\ell} \cdot \boldsymbol{\nabla} S}, \tag{7}$$

where $\hat{\ell}$ is the direction along which the cut is taken.

In two dimensions, we define a complex density ratio, which does not depend on any particular direction, as

$$R \equiv \frac{\partial_x T + i\partial_y T}{\partial_x S + i\partial_y S}, \text{ where } \quad i \equiv \sqrt{-1}. \tag{8}$$

The phase ϕ of the complex density ratio R quantifies the degree of alignment of the T and S gradients. If the phase is $\phi = 0°$ or $\phi = 180°$, then there is *thermohaline alignment* and the definition of R in the complex plane is equivalent to that in (7), regardless of the orientation of $\hat{\ell}$. The magnitude of R quantifies the relative strength of the gradients of T and S. If $|R| = 1$ and $\phi = 0°$, then temperature and salinity cancel each other in the buoyancy balance and there is *thermohaline compensation*. Thermohaline gradients for which $|R| > 1$ are *temperature dominated*, while those for which $|R| < 1$ are *salinity dominated*.

Together with R, it is useful to introduce the Turner angle, $\mathrm{Tu} \equiv \arctan |R|$. We choose the branch of the arctangent such that $0 \le \mathrm{Tu} \le \pi/2$. Temperature-dominated gradients are mapped into $\pi/4 \le \mathrm{Tu} \le \pi/2$ and salinity dominated gradients into $0 \le \mathrm{Tu} \le \pi/4$. In the following we use the joint PDF $\mathcal{P}(\mathrm{Tu}, \phi)$ to describe the degree of alignment and compensation of the ML. The joint PDF is normalized according to

$$\int_0^{\pi/2} d\mathrm{Tu} \int_0^{2\pi} d\phi\, \mathcal{P}(\mathrm{Tu}, \phi) = 1. \tag{9}$$

a. Alignment

We now use R and Tu to study the correlations that develop between the temperature and salinity gradients in the ML. The effect of horizontal stirring on the gradients is better understood by neglecting the right-hand side of (4) and (5). In this limit the thermohaline Jacobian $\mathcal{J} \equiv J(T, S)$ becomes a material invariant (Young 1994). However stirring tends, on average, to increase the gradients of advected scalars. Thus $\boldsymbol{\nabla} T$ and $\boldsymbol{\nabla} S$ become parallel ($\phi = 0°$) or antiparallel ($\phi = 180°$) in order to preserve the constancy of the Jacobian $\mathcal{J} = |\boldsymbol{\nabla} T||\boldsymbol{\nabla} S| \sin\phi$.

Alignment will also appear in the presence of forcing and linear dissipation if it can be established on a timescale shorter than that on which diffusion arrests the growth of thermohaline gradients. Provided that the tracers are forced at scales larger than the eddy scale L_0, we can estimate both timescales in 2D turbulence. Lapeyre et al. (1999) show that the typical time for the process of alignment is given by the inverse of the local rate of strain $t_{\mathrm{align}} \approx \sigma^{-1}$. In the direction along which the tracer isolines are compressed, the scales of the fluctuations decrease as $\exp(-\sigma t)$ (Ottino 1988). The exponential contraction continues until the cascade is halted by linear diffusion at the dissipation scale L_{diss}. Thus compression is arrested after a time:

$$t_{\mathrm{diss}} \approx \sigma^{-1} \ln(L_0/L_{\mathrm{diss}}). \tag{10}$$

In Fig. 1a, we show the time-averaged joint PDF $\mathcal{P}(\mathrm{Tu}, \phi)$ for simulation L1 (cf. Table 1), where temperature and salinity are advected and diffused independently of each other, and a Laplacian diffusion operator is used instead of the nonlinear diffusion. The scale of the stirring forcing is $L_0 = 6.4$ km and the dissipation scale is $L_{\mathrm{diss}} \approx 0.23$ km. Then $t_{\mathrm{align}} < t_{\mathrm{diss}}$ and alignment can be established. In Fig. 1b, we show the result from simulation L2 (cf. Table 1), in all respects identical to simulation L1 except that the forcing scale of the stirring field is set to $L_0 = 0.3$ km. In this second example, $t_{\mathrm{align}} \approx t_{\mathrm{diss}}$ and the joint PDF of $\mathcal{P}(\mathrm{Tu}, \phi)$ is quite spread; that is, the gradients of T and S are not well aligned.

Note that, in the absence of nonlinear diffusion, stirring creates thermohaline alignment but not thermohaline compensation. In simulation L1 there is no preference for parallel versus antiparallel gradients. Stirring however affects the PDF of the Turner angle. When the separation between the forcing and the dissipation scale allows for an effective alignment process, as in simulation L1, the highest probability is at $\mathrm{Tu} = \pi/4$, $\phi = 0°$ and $\mathrm{Tu} = \pi/4$, $\phi = 180°$. Values of $\mathrm{Tu} = \pi/4$ appear more often than values close to 0 and $\pi/2$, because the largest values of $|\boldsymbol{\nabla} T|$ and $|\boldsymbol{\nabla} S|$ are most likely to occur at the same position, in regions of large strain.

b. Compensation

We now show the action of nonlinear diffusion by solving (4) and (5) while forcing T and S along parallel bands (cf. Table 1, simulation NL1). In this way, all values of Tu are created with the same probability at angles $\phi = 0°$ and $\phi = 180°$.

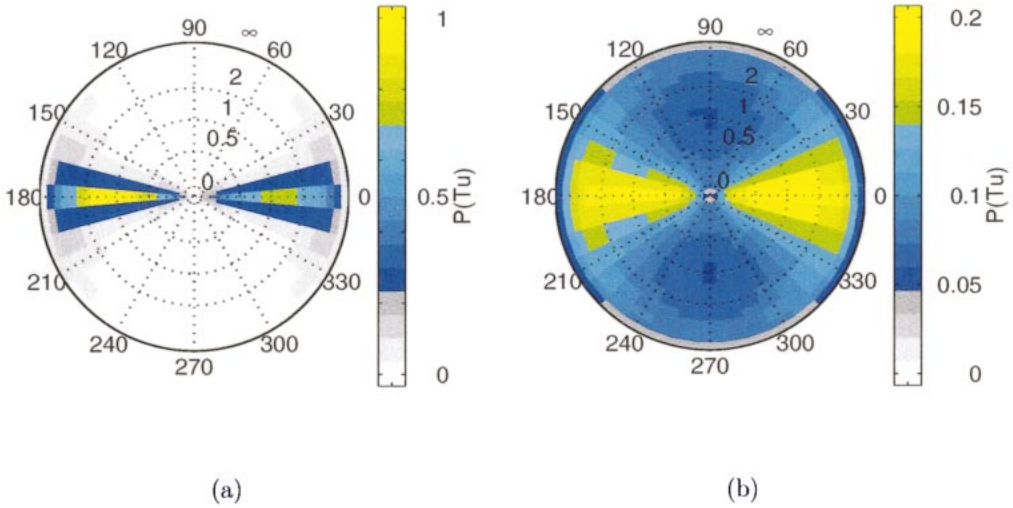

FIG. 1. Joint PDF $\mathcal{P}(\mathrm{Tu}, \phi)$ of the complex density ratio R defined in (8). The azimuthal position in the radar plot indicates the angle between the temperature and the salinity gradients, while the radial displacement is the ratio of their magnitudes. The PDF is an average over 300 h during which the simulation was in equilibrium. (a) Simulation L1: the forcing on vorticity is at 6.4 km; nearly all points lie along the angles of alignment, i.e., at angles $\phi = 0°$ and $\phi = 180°$. (b) Simulation L2: the forcing on vorticity is at 300 m; points are quite spread and there is only a very weak tendency for alignment. Note the different color scale in the two panels.

The large-scale patterns of B and V, in Fig. 2, reflect the sinusoidal structure of the forcing. At small scales the two fields are remarkably different. Sharp spice gradients with little or no signature in buoyancy are the signature of thermohaline compensation. The corresponding temperature and salinity fields in a small square of $(10\ \mathrm{km})^2$ are shown in Fig. 3. Temperature and salinity gradients are quite similar and oppose in their joint effect on buoyancy. In Fig. 4a we show the time-averaged joint PDF $\mathcal{P}(\mathrm{Tu}, \phi)$. The joint PDF has a single, sharp maximum at $\mathrm{Tu} = \pi/4$ and $\phi = 0°$, indicating a strong tendency for compensation. A comparison with the case of Fig. 1a shows that nonlinear diffusion selectively dissipates all gradients whose Tu is different from $\pi/4$ and $\phi = 0°$. Compensation is not maintained at all times though. There are moments when the PDF develops other maxima. This happens when the stirring field momentarily creates large buoyancy gradients at small scales. However these buoyancy anomalies are quickly dissipated by nonlinear diffusion.

We also considered the case where the forcings on T and S act along orthogonal directions with different strengths (cf. Table 1, simulation NL2). Once again, all values of Tu are created by the forcing, but there is now a strong bias toward $\mathrm{Tu} = \arctan(2)$. Compensation is established through a two step process: advection generates aligned, small-scale gradients by deforming the orthogonal, large-scale patterns created by the forcing and nonlinear diffusion eliminates all the small-scale gradients with Tu different from $\pi/4$. Compensated gradients are not created in this process; rather, they remain after the noncompensated ones are dissipated. In Fig. 4b we show the time-averaged joint PDF $\mathcal{P}(\mathrm{Tu}, \phi)$ for this run: it is skewed toward the right half of the radar plot, indicating a tendency toward compensation. However, it has two maxima, one at $\mathrm{Tu} = \pi/4$ and the other at $\mathrm{Tu} = \arctan(2)$, along the line $\phi° = 0$. Nonlinear diffusion successfully selects compensated gradients, but it cannot erase completely the action of the forcing that continuously creates gradients with $\mathrm{Tu} = \arctan(2)$.

c. Compensation as a function of spatial scales

The temperature–salinity relationship in the simulations described above changes as a function of spatial scale. At large scales, temperature and salinity evolve independently and relax to the profiles imposed by the forcing. At small scales, nonlinear diffusion is effective at removing buoyancy variance and creates correlations in the form of thermohaline compensation. This scale-dependence is well described by the differences in the spectra of buoyancy $E_B(k)$ and spice $E_V(k)$. In Fig. 5, we show the time-averaged spectra for simulation NL1 as a function of the radial wavenumber $k = \sqrt{k_x^2 + k_y^2}$. Spice is more energetic than buoyancy at small scales (large wavenumbers), as expected if spice gradients are larger than buoyancy gradients. The spectral gap disappears at large scales.

An offset between the spectral levels of buoyancy and spice is consistent with the observations of Ferrari and Rudnick (2000). However, buoyancy spectra in the ocean ML roll off as k^{-2}, while the spectrum in Fig. 5 has a slope close to k^{-5}. We can rule out the hypothesis that this difference is the result of our idealized stirring field, by deriving a scaling law that relates the slope of the buoyancy spectrum $E_B(k)$ to the slope of the kinetic energy spectrum $\mathcal{E}(k)$ of the advecting field.

Let us call $\mathcal{B}(l)$ the characteristic buoyancy fluctua-

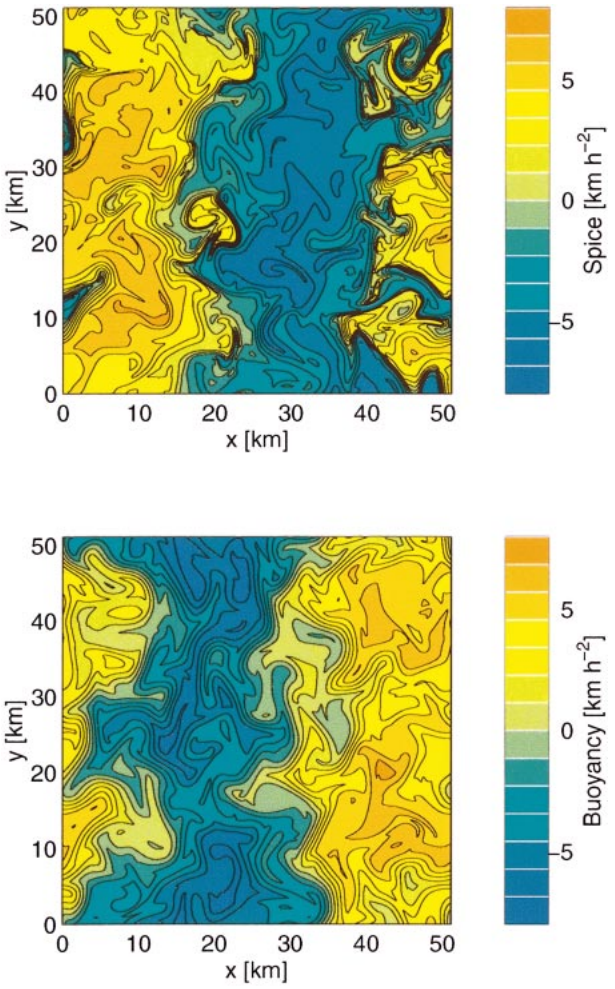

FIG. 2. Snapshots of spice and buoyancy from simulation NL1 at $t = 700$ h.

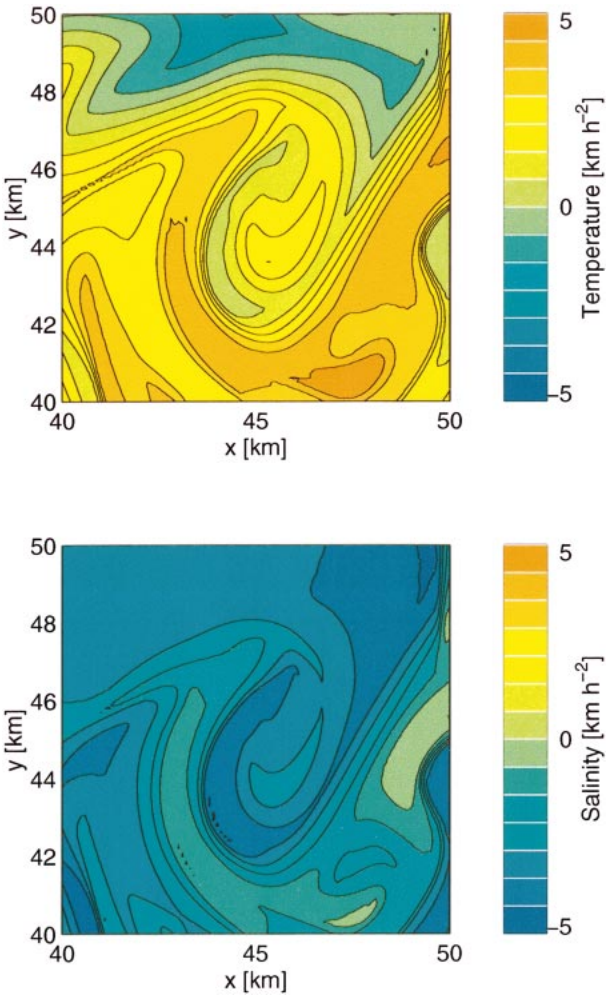

FIG. 3. A blowup of temperature and salinity corresponding to the B and V shown in Fig. 2. Notice that T and S contours are very similar at small scales both in spacing and in orientation.

tion at a scale l. This amount of buoyancy is fluxed to smaller scales by stirring in a time determined as the inverse of the average strain rate acting on buoyancy patches of size l, namely,

$$\sigma(l) \propto \sqrt{\int_{k_0}^{k} k^2 \mathcal{E}(k)\, dk}. \tag{11}$$

Here $k = 2\pi/l$. The spectrum of energy $\mathcal{E}(k)$ is assumed as given and k_0 is a lower wavenumber cutoff below which $\mathcal{E}(k)$ vanishes. Applying this scaling to the nonlinear diffusion equation for buoyancy in (4) gives

$$\sigma(l)\mathcal{B}(l) \sim \gamma \frac{\mathcal{B}^3(l)}{l^4}, \tag{12}$$

under the assumption that the system is in statistical equilibrium and external forcing does not act directly on scale l.

There are now two possibilities: 1) If the velocity field is characterized by nonlocal dynamics in the spectral domain, that is, if $\mathcal{E}(k)$ rolls off faster than k^{-3} below some energy-containing wavenumber k_0, then the integral in (11) is dominated by contributions from wavenumber k_0 and the strain rate is independent of the scale l, $\sigma(l) = \sigma_0$. The scaling law in (12) becomes

$$\mathcal{B}^2 \sim \frac{\sigma_0}{\gamma} l^4,$$

which can be converted in the wavenumber domain to obtain the buoyancy spectral density,

$$E_B \propto \frac{\sigma_0}{\gamma} k^{-5}. \tag{13}$$

2) If the velocity field has a spectral slope $k^{-\alpha}$ with α between -3 and -1, dynamics are local in wavenumber space and the strain rate is dominated at every scale by energy at that scale. Estimating the integral in (11) and substituting in (12) gives $E_B \propto (\epsilon_0/\gamma)k^{-(\alpha+7)/2}$; that is,

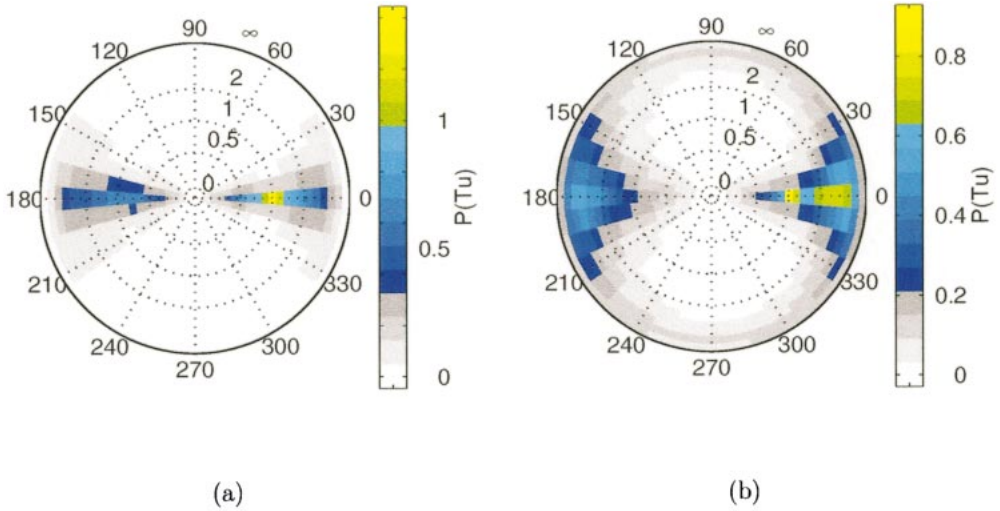

FIG. 4. Joint PDF $\mathcal{P}(\mathrm{Tu}, \phi)$ of the complex density ratio R, calculated as explained for Fig. 1. (a) Simulation NL1: there is a clear peak at $R = 1$, evident as a yellow spot, indicating that most thermohaline gradients are compensated. (b) Simulation NL3: the large-scale forcing on temperature has 2 times the amplitude of that on salinity, but the maximum of the PDF is at $R = 1$; values of R close to 2 are much more likely in this simulation than in (a) because nonlinear diffusion selects compensation but does not remove completely the asymmetry in the large-scale forcing.

the spectrum of buoyancy has a slope between -5 and -4.

We tested the scaling by running simulations in which the forcing on vorticity was applied at small (0.3 km) and large (6.4 km) scales. The kinetic energy spectra had respectively slopes of $k^{-1.3}$ (inverse energy cascade) and $k^{-3.8}$ (direct enstrophy cascade), and so we could test the scaling both for local and nonlocal regimes. The corresponding spectra of buoyancy developed spectral slopes of $k^{-4.15}$ and k^{-5} in agreement with the scaling just derived (Figs. 5 and 6).

Velocity spectra in the ocean ML on scales between 1 and 10 km appear to have spectral slopes close to k^{-2} (e.g., Sutton 2001). According to our scaling, such a stirring filed would produce buoyancy spectra with a slope of $k^{-4.5}$, in disagreement with the observed k^{-2}. This suggests that in the real ocean spectral slopes of T and S are not set by a simple balance between nonlinear diffusion and advection, but other processes come into play. We come back to this point in the conclusions.

A final point of interest for the real ocean is what sets the largest scale below which compensation is ob-

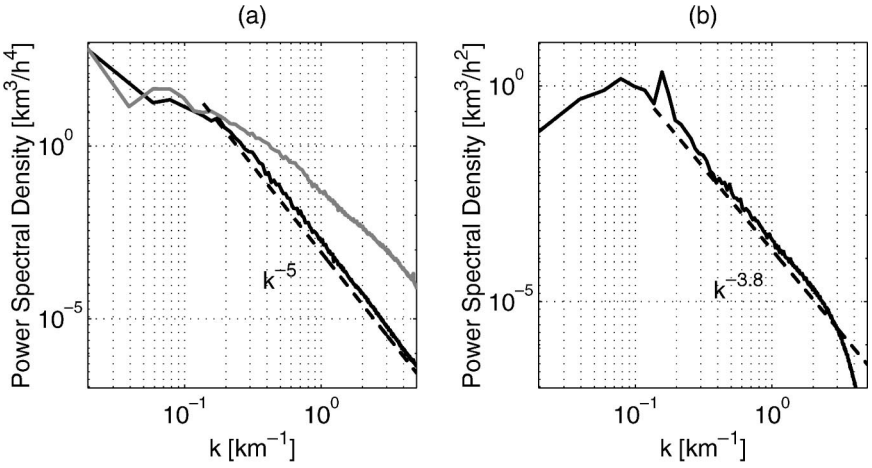

FIG. 5. (a) Isotropic spectrum of buoyancy (black line) and spice (gray line) for simulation NL1. (b) Isotropic spectrum of energy. The slope of the spectrum of energy, computed with a least squares fit, is consistent with previous result from numerical simulations of two-dimensional turbulence in the direct enstrophy cascade regime. The slope of the spectrum of buoyancy is predicted by scaling arguments given in the text.

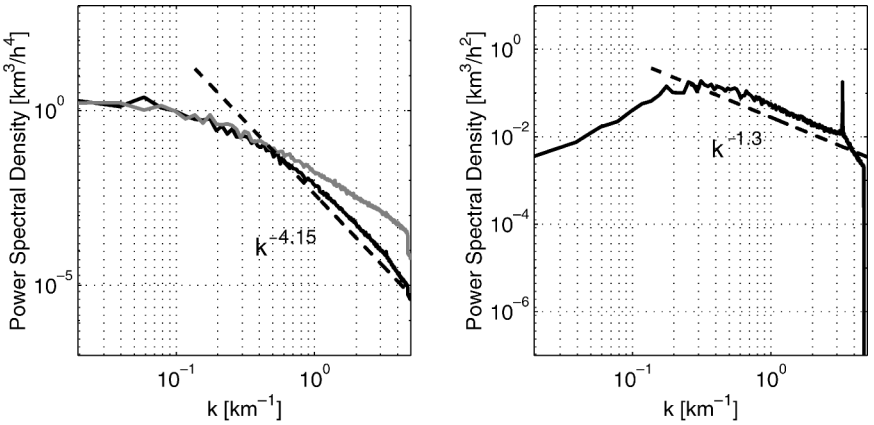

FIG. 6. (a) Isotropic spectrum of buoyancy (black line) and spice (gray line) for simulation NL3. (b) Isotropic spectrum of energy. The slope of the spectrum of energy, computed with a least squares fit, is consistent with previous result from numerical simulations of two-dimensional turbulence in the inverse energy cascade regime. The slope of the spectrum of buoyancy is predicted by scaling arguments given in the text.

served. An analysis of the variance budget for buoyancy provides an answer in our simple model. Let us multiply (4) by B and average over the whole domain and over several turnover times. In equilibrium, we have

$$\langle \mathcal{F}_B B \rangle = \gamma \langle |\nabla B|^4 \rangle. \tag{14}$$

The term on the left-hand side is the injection of buoyancy variance from the forcing. In our simulations variance is injected at the domain scale, where nonlinear diffusion is negligible: the product $\langle \mathcal{F}_B B \rangle$ depends only on the large-scale structure of B. The term on the right-hand side is equal to the total variance dissipated by nonlinear diffusion. The buoyancy gradient that appears in this term is the result of the superposition of buoyancy fluctuations on a range of scales, which must be as wide as to match the total variance injected by forcing and stirring at the largest scales, thus satisfying (14).

To gain some insight on this mechanism, we have performed a series of computations with different values of γ ranging from 2×10^{-3} to 2×10^{-1} km^2 h^{-3} (simulations NL4–NL8 in Table 1). To limit the computational cost, these simulations have been performed with 128×128 grid points, corresponding to a domain of 12.8×12.8 km. Vorticity is forced at a scale of 1 km. Buoyancy and spice are forced at the lowest wavenumber (which now corresponds to a scale 12.8 km), with the same geometry used in simulation NL1. The buoyancy spectra for these simulations are shown in Fig. 7a. At the lowest wavenumber all spectra converge to a common value, and at high wavenumbers they nicely

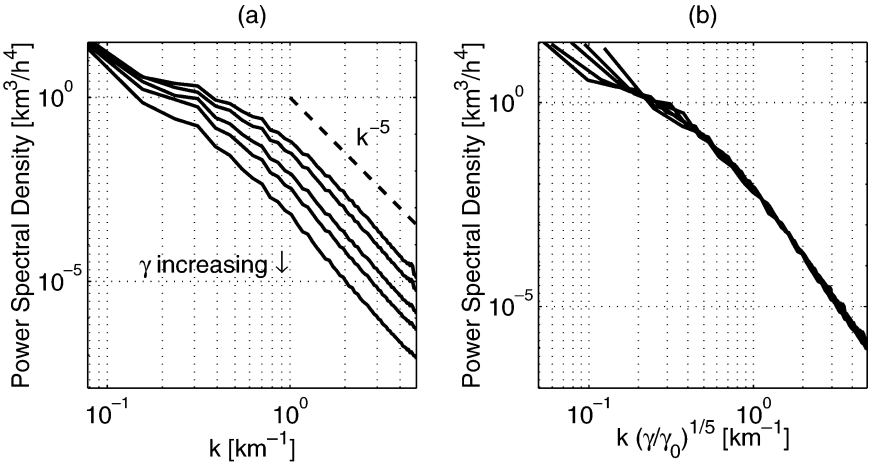

FIG. 7. (a) Spectra of buoyancy from a set of simulations, NL4–NL8, run with $N = 128$ points. The spectral level of buoyancy decreases with increasing γ but maintains the same spectral slope in the scaling region. Notice that all spectra converge at the lowest wavenumber. (b) The buoyancy spectra for different γ collapsed according to the scaling law described in the text. We set $\gamma_0 = 0.02$ km^2 h^3.

follow the k^{-5} scaling. However, in the scaling regime, the spectra are offset and lower energy levels correspond to higher values of γ. The scaling in (13) predicts that the ratio between the spectra should be proportional to γ^{-1} or equivalently that all spectra should collapse if plotted versus $k/\gamma^{1/5}$, in the wavenumber range where the scaling holds. This is verified in Fig. 7.

The scaling in (13) suggests that, as γ increases, the amount of variance at a given wavenumber decreases. Thus the range of scales over which nonlinear diffusion acts has to extend to lower wavenumbers in order to satisfy the constraint in (14).

A dependence of compensation on γ is consistent with observations. Rudnick and Martin (2002) find compensation on scales of 3 km only when the vertical turbulent mixing in the ML is strong. In our simple model γ is a proxy for the strength of vertical turbulent processes (Ferrari and Young 1997). Thus the model successfully predicts that an increase (decrease) in turbulent mixing extends (shrinks) the range of scales below which compensation is established.

5. Conclusions

We have shown that a simple, idealized model of the mesoscale dynamics of the ML reproduces the compensation and thermohaline alignment observed in the real ocean at scales shorter than 10 km (Ferrari and Rudnick 2000). Compensation is the result of preferential diffusion of horizontal buoyancy gradients, which occurs because unbalanced motions due to these gradients are stronger in the ML than in the more nearly geostrophic interior. A novel result of this paper is that compensation is maintained also in the presence of the mesoscale motions and thermohaline forcing that act in the ML. Actually, the preferential diffusion of buoyancy gradients is enhanced by the mesoscale stirring field: the mesoscale strain exponentially increases buoyancy gradients until they become gravitationally unstable and are mixed away. Simulations confirm that, at any single time, one only rarely encounters buoyancy gradients. Temperature and salinity are typically compensated, in agreement with observations.

Our model provides a simple explanation for the alignment and compensation of thermohaline gradients but fails to reproduce the temperature and salinity spectral laws observed in the oceanic ML. This disagreement suggests that dynamical balances different from those explored in this paper are responsible for the maintenance of the spectral slopes observed in nature. Two candidates come to mind. First, nonlinear diffusion acts best in the presence of strong vertical mixing in the ML. Alignment and compensation is established during these times of intense mixing, such as in the presence of strong atmospheric forcing. The rest of the time nonlinear diffusion becomes weak and all diffusion processes are negligible down to scales of a few hundred meters. In this regime horizontal stirring cannot destroy compensation, because that would require differential advection of heat and salt, but it can redistribute thermohaline variance across wavenumbers. Current theories of turbulence (Salmon 1998) suggest that the observed k^{-2} spectra of T and S can be maintained by a horizontal kinetic energy spectrum with a slope of k^{-1}. Velocity measurements on spatial scales between 100 m and 10 km are not presently available to test this hypothesis.

Second, air–sea fluxes have a broad spatial spectrum and can modify the spectral slopes of temperature and salinity in the ML. In this paper we represented thermohaline forcing as a large-scale process, with no small-scale content. It would be very interesting to extend this study to explore the importance of the spectral characteristic of air–sea fluxes for the thermohaline structure of the ML. However there are no measurements of T, S, and air–sea fluxes on small scales to test the results of such an investigation. All that is available from data is the evidence of thermohaline alignment and compensation on scales below 10 km. Explaining this observation was the main focus of this research.

We believe that this work has important implications for numerical models of the ML. Traditionally a large effort has been placed in improving parameterizations of the turbulent fluxes that homogenize vertically the ML. Comparatively little research has been done into understanding the ML dynamics on short horizontal scales. However, we have shown that a proper parameterization of horizontal mixing of buoyancy gradients on submesoscales is necessary to reproduce observations. To the authors' knowledge, no numerical model for the study of the ocean circulation includes parameterizations for this process. As a result there might be biases between model outputs and observations in the thermohaline structure of the upper ocean.

Acknowledgments. We thank W. Young and D. Rudnick for helpful discussions. Part of the work was done in Woods Hole during the GFD summer school of 2001. Author R. Ferrari acknowledges the support of the National Science Foundation (OCE96-16017) and the WHOI Postdoctoral Fellowship. Author F. Paparella was supported by the Department of Energy through the Climate Change Prediction Program.

REFERENCES

Belkin, I. M., 1996: Southern Ocean fronts from the Greenwich meridian to Tasmania. *J. Geophys. Res.*, **101,** 3675–3696.

Canuto, C., M. Y. Hussaini, A. Quarteroni, and T. A. Zang, 1987: *Spectral Methods in Fluid Dynamics.* Springer-Verlag, 567 pp.

Ferrari, R., and W. R. Young, 1997: On the development of thermohaline correlations as a result of nonlinear diffusive parameterizations. *J. Mar. Res.,* **55,** 1069–1101.

——, and D. L. Rudnick, 2000: Thermohaline structure of the upper ocean. *J. Geophys. Res.,* **105C,** 16 857–16 883.

Flament, P., L. Armi, and L. Washburn, 1985: The evolving structure of an upwelling filament. *J. Geophys. Res.,* **90,** 11 765–11 778.

Green, J. A., 1970: Transfer properties of the large-scale eddies and

the general circulation of the atmosphere. *Quart. J. Roy. Meteor. Soc.*, **96,** 157–185.

Lapeyre, G., P. Klein, and B. L. Hua, 1999: Does the gradient vector align with the strain eigenvector in 2D turbulence? *Phys. Fluids*, **11,** 3729–3737.

Munk, W., 1981: Internal waves and small-scale processes. *Evolution of Physical Oceanography*, B. A. Warren and C. Wunsch, Eds., MIT Press, 264–291.

Niiler, P. P., 1984: The three-dimensional circulation near the eastern North Pacific Subtropical Front. *J. Phys. Oceanogr.*, **14,** 217–230.

Ottino, J. M., 1988: *The Kinematics of Mixing: Stretching, Chaos, and Transport.* Cambridge University Press, 354 pp.

Pavan, V., and I. Held, 1996: The diffusive approximation for eddy fluxes in baroclinically unstable jets. *J. Atmos. Sci.*, **53,** 1262–1272.

Roden, G. I., 1975: On North Pacific temperature, salinity, sound velocity and density fronts and their relation to the wind and energy flux fields. *J. Phys. Oceanogr.*, **5,** 557–571.

——, 1977: Oceanic subarctic fronts of the Central Pacific: Structure of and response to atmospheric forcing. *J. Phys. Oceanogr.*, **7,** 761–778.

Rudnick, D. L., and J. R. Luyten, 1996: Intensive surveys of the Azores Front. 1: Tracers and dynamics. *J. Geophys. Res.*, **101,** 923–939.

——, and R. Ferrari, 1999: Compensation of horizontal temperature and salinity gradients in the ocean mixed layer. *Science*, **283,** 526–529.

——, and J. R. Martin, 2002: On the horizontal density ratio in the upper ocean. *Dyn. Atmos. Oceans*, **36,** 3–21.

Salmon, R. L., 1998: *Lectures on Geophysical Fluid Dynamics.* Oxford University Press, 378 pp.

Stone, P. H., 1972: A simplified radiative–dynamical model for the static stability of rotating atmospheres. *J. Atmos. Sci.*, **29,** 157–185.

Sutton, P., 2001: Detailed structure of the Subtropical Front over Chatham Rise, east of New Zealand. *J. Geophys. Res.*, **106,** 31 045–31 056.

Veronis, G., 1972: On properties of seawater defined by temperature, salinity and pressure. *J. Mar. Res.*, **30,** 227–255.

Visbeck, M., J. Marshall, T. Haine, and M. A. Spall, 1997: Specification of eddy transfer coefficients in coarse-resolution ocean circulation models. *J. Phys. Oceanogr.*, **27,** 381–402.

Young, W. R., 1994: The subinertial mixed layer approximation. *J. Phys. Oceanogr.*, **24,** 1812–1826.